nature neuroscience

ARTICLES

Calmodulin as a direct detector of Ca^{2+} signals

Guido C Faas[1], Sridhar Raghavachari[2], John E Lisman[3] & Istvan Mody[1,4]

Many forms of signal transduction occur when Ca^{2+} enters the cytoplasm of a cell. It has been generally thought that there is a fast buffer that rapidly reduces the free Ca^{2+} level and that it is this buffered level of Ca^{2+} that triggers downstream biochemical processes, notably the activation of calmodulin (CaM) and the resulting activation of CaM-dependent enzymes. Given the importance of these transduction processes, it is crucial to understand exactly how Ca^{2+} activates CaM. We have determined the rate at which Ca^{2+} binds to CaM and found that Ca^{2+} binds more rapidly to CaM than to other Ca^{2+}-binding proteins. This property of CaM and its high concentration support a new view of signal transduction: CaM directly intercepts incoming Ca^{2+} and sets the free Ca^{2+} level (that is, it strongly contributes to fast Ca^{2+} buffering) rather than responding to the lower Ca^{2+} level set by other buffers. This property is crucial for making CaM an efficient transducer. Our results also suggest that other Ca^{2+} binding proteins have a previously undescribed role in regulating the lifetime of Ca^{2+} bound to CaM and thereby setting the gain of signal transduction.

Given the key role of CaM in transduction[1–3] and Ca^{2+} dynamics[4], it is essential to understand the kinetics of Ca^{2+} binding to CaM. There are two Ca^{2+}-binding sites at the N terminus of CaM and two at the C terminus (N- and C-lobes). These sites have distinct Ca^{2+}-binding properties[5,6]. Previous work has inferred on-rate constants (k_{on} values) from measurements of off-rate constants (k_{off} values) and used stopped-flow fluorimetry, a method with a relatively long dead time (>2 ms) that precludes accurate determination of the fast kinetics of the N-lobe[4,7,8]. We measured the binding more directly by determining the fall in $[Ca^{2+}]_{free}$ after a rapid (<100 µs) $\Delta[Ca^{2+}]_{total}$ produced by flash photolysis of DM-nitrophen (DMn)[9–11]. We found that the N-lobe of CaM binds Ca^{2+} faster than previously determined for any calcium-binding protein (CBP). Thus the N-lobe is the first site of cellular Ca^{2+} binding. Furthermore, the cooperativity of Ca^{2+} binding differs between the two lobes and this difference gives rise to distinct properties of each lobe. Our findings show that CaM is efficiently activated upon a rise in cellular Ca^{2+}, which might produce 10–100 times more activated CaM than previously thought.

RESULTS

The Ca^{2+} binding kinetics of CaM

We determined the binding kinetics of CaM *in vitro* by rapidly (<100 µs) uncaging Ca^{2+} from DMn in the presence of CaM. The uncaged Ca^{2+} is quickly bound by CaM. We measured the $[Ca^{2+}]$ dynamics with a fast fluorescent Ca^{2+} indicator (Oregon Green BAPTA 5N, OGB-5N; see Online Methods) that was also present in the reaction chamber. By analyzing the data with a model that simulates all reactions that occur in the chamber, we derived the Ca^{2+} binding kinetics of CaM[9–11] (see Online Methods). At a near physiological temperature (35 °C) with 47–187 µM CaM present, the decay in $[Ca^{2+}]$ had multiple time constants (**Fig. 1a**). To quantify the binding kinetics, we fitted the data with a two-step binding model of cooperative binding to each lobe[11] (see Online Methods and **Supplementary Figs. 1–6**):

$$N_TN_T + Ca^{2+} \underset{k_{off(T),N}}{\overset{2 \times k_{on(T),N}}{\rightleftharpoons}} CaN_TN_R + Ca^{2+} \underset{2 \times k_{off(R),N}}{\overset{k_{on(R),N}}{\rightleftharpoons}} CaN_RCaN_R \quad (1)$$

$$C_TC_T + Ca^{2+} \underset{k_{off(T),C}}{\overset{2 \times k_{on(T),C}}{\rightleftharpoons}} CaC_TC_R + Ca^{2+} \underset{2 \times k_{off(R),C}}{\overset{k_{on(R),C}}{\rightleftharpoons}} CaC_RCaC_R \quad (2)$$

where N_x and C_x represent binding sites on the N and C lobes, respectively; after the first binding, the state changes from T to R, giving rise to cooperativity[11] (**Supplementary Fig. 2**). The model had to correctly fit data that were measured over a wide range of experimental conditions. This strongly constrained the fits and assured that accurate kinetics were determined (see Online Methods). To understand the role of each lobe, we also used CaM mutants in which Ca^{2+} could not bind to either the N-lobe or the C-lobe.

The fits (**Table 1**) reliably described the data (**Supplementary Figs. 1–6**) and were consistent with previous work[5,6] showing that the C-lobe bound Ca^{2+} with higher affinity than the N-lobe (**Fig. 1b**). Our findings provide two insights that are, to our knowledge, new. First, both lobes showed cooperativity, but by different mechanisms. The T-to-R transition strongly increased (~40×) k_{on} for Ca^{2+} binding to the N-lobe and modestly decreased k_{off} (~1/7) By contrast, k_{on} of the C-lobe was changed little by the T-to-R

[1]Department of Neurology, University of California Los Angeles, Los Angeles, California, USA. [2]Department of Neurobiology, Duke University, Durham, North Carolina, USA. [3]Department of Biology, Brandeis University, Waltham, Massachusetts, USA. [4]Department of Physiology, University of California Los Angeles, Los Angeles, California, USA. Correspondence should be addressed to G.C.F. (gfaas@ucla.edu).

Received 7 October 2010; accepted 22 December 2010; published online 23 January 2011; doi:10.1038/nn.2746

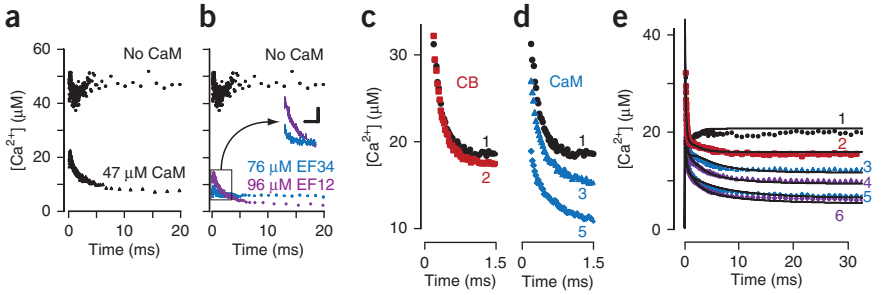

Figure 1 Ca^{2+} buffering by CaM and the different roles of CaM and CB. (**a**,**b**) Step in $[Ca^{2+}]_{free}$ as a flash uncages Ca^{2+} bound to DMn (~4.5% of 3.6 mM DMn is uncaged, baseline $[Ca^{2+}]_{free}$ = ~500 nM (dashed line)[10]). (**a**) When CaM is present, the released Ca^{2+} is buffered in at least two phases. Initially, a large part is buffered very rapidly, as indicated by the low $[Ca^{2+}]_{peak}$. This is followed by a slower decay phase. (**b**) With a CaM mutant in which only the N-lobe binds Ca^{2+} (CaM_{EF34}), only a fast component is apparent. With a CaM mutant in which only the C-lobe binds Ca^{2+} (CaM_{EF12}), even a higher concentration produces less initial buffering, but the slow component is evident. Inset shows initial CaM trace at 2× larger scale. (**c**–**e**) Ca^{2+} transients produced by uncaging 6–7% of 3.6 mM DMn (baseline ~300 nM $[Ca^{2+}]_{free}$). (**c**) When calbindin (CB; red, trace 2) is added, initial Ca^{2+} dynamics are unchanged compared to control (black, trace 1). (**d**) Addition of CaM increases the fast buffering (adding to the initial rapid reduction caused by DMn alone) (blue; trace 3, 13 μM; trace 5, 26 μM). (**e**) With CaM present, addition of calbindin increases the slow reduction (purple; trace 4, 34 μM calbindin + 13 μM CaM; trace 6, 34 μM calbindin + 26 μM CaM). All data in the mixtures could be closely fit with a mathematical model (solid black lines) using the kinetics of CaM and calbindin.

transition; cooperativity arose from a ~1/400 decrease in k_{off}, consistent with previous experiments[4,7,8]. Second, the absolute rate of Ca^{2+} binding to the N-lobe was very fast: the T state had a k_{on} of 7.7×10^8 M^{-1} s^{-1}, faster than previous indirect estimates of 2.5–5 × 10^8 M^{-1} s^{-1} (refs. 4,8). In addition, the R state has a k_{on} of 3.2×10^{10} M^{-1} s^{-1}, which greatly exceeds previous indirect estimates[4,7,8] but is within the diffusion-limited speed (see **Supplementary Data 1**).

CA1 pyramidal cells have served as a model system for understanding Ca^{2+} dynamics and the role of Ca^{2+} buffers. A major CBP in these cells is calbindin[12]. We measured the properties of calbindin at 35 °C (**Table 1** and **Supplementary Fig. 4**) and found that they were comparable to earlier measurements[9,12] (the small discrepancies can be explained by differences in experimental conditions; see **Supplementary Data 2**). Although calbindin is generally considered to be a relatively fast Ca^{2+} buffer, it is two orders of magnitude slower than the N-lobe of CaM in the R state.

To understand the implications of these extremely different binding rates, we measured Ca^{2+} dynamics in uncaging experiments with both buffers present (**Fig. 1c**–**e**). Immediately (<100 μs) after uncaging, Ca^{2+}_{free} became bound to CaM (**Fig. 1d**), well before being bound to calbindin (**Fig. 1c**), which shows that CaM is a faster buffer than calbindin. Furthermore, the combined action of CaM and calbindin produced a slower buffering component that was additive when both proteins were present (**Fig. 1e**). A simple computational model based on the properties of CaM, calbindin and DMn (which also acts as a Ca^{2+} buffer) accounts for the Ca^{2+} dynamics in the mixture (**Fig. 1e**). Although these experiments are done at levels of basal $[Ca^{2+}]_{free}$ higher than the physiological range (this is necessary to keep DMn loaded with Ca^{2+}), the resulting model, with a more realistic $[Ca^{2+}]_{free}$ and without DMn, can be used to understand Ca^{2+} dynamics under physiological conditions (see below).

Ca^{2+} buffering by CaM in spines

In dendritic spines of hippocampal CA1 pyramidal cells, Ca^{2+} entry during an action potential elevates $[Ca^{2+}]_{total}$ by ~50 μM, but the measured rise is only a few μM owing to the action of fast buffers[13,14]. This buffering action is described by the 'buffering capacity' κ (usually measured as the total $\Delta[Ca^{2+}]$ that remains undetected by the Ca^{2+} indicator owing to fast buffering, relative to the $\Delta[Ca^{2+}]$ that is detected by the Ca^{2+} indicator; see **Supplementary Data 3**). We simulated how CaM (100 μM (refs. 15,16); see **Supplementary Data 4** and **Supplementary Table 1**) and calbindin (30 μM (ref. 17)) affected κ (at $[Ca^{2+}]_{rest}$ = 100 nM). The $[Ca^{2+}]$ measured with negligible OGB-1 ($[Ca^{2+}]_{OGB\text{-}1}$) is the $[Ca^{2+}]$ as it would be determined with the 'added buffer' method[18–20]. The computed peak $[Ca^{2+}]_{OGB\text{-}1}$ is 2.5 μM during an action potential (**Fig. 2a**), yielding κ = 19 (see **Supplementary Data 5**). This buffering capacity is consistent with measurements in dendritic spines (~20)[13,14]. It has been suggested that ATP, which can bind Ca^{2+} when not complexed with Mg^{2+}, might also contribute to fast Ca^{2+} buffering[21]. However, our calculations show that in the presence of CaM, addition of ATP (4 mM (ref. 21)) increased κ at most by 5%, indicating that ATP makes a minimal contribution to fast buffering (see **Supplementary Data 6** and **Supplementary Fig. 7**). These findings are consistent with the idea that CaM is the main fast Ca^{2+} buffer in spines. One property of the fast buffer is that it does

Table 1 Ca^{2+} binding properties of CaM and calbindin

		N terminus		C terminus		
		CaM_{WT} (high $k_{d(app)}$)	CaM_{EF34}	CaM_{WT} (low $k_{d(app)}$)	CaM_{EF12}	Calbindin
	Conditions	7	4	7	4	10
n	Traces	94	52	94	51	150
	n (fit sets)	32	26	32	30	30
$k_{d(T)}$	log M (μM)	–3.7 ± 0.3 (193)	–3.1 ± 0.6 (641)	–4.6 ± 0.2 (27.8)	–4.1 ± 0.4 (86.9)	–6.4 ± 0.2 (0.393)
$k_{d(R)}$	log M (μM)	–6.1 ± 0.3 (0.788)	–6.8 ± 0.6 (0.138)	–6.6 ± 0.3 (0.264)	–6.5 ± 0.3 (0.261)	
$k_{d(app)}$	log M (μM)	–4.9 ± 0.1 (12.7)	–5.0 ± 0.0 (9.2)	–5.6 ± 0.2 (2.7)	–5.3 ± 0.1 (4.8)	
n_H		1.9 ± 0.1	2.0 ± 0.0	1.8 ± 0.1	1.9 ± 0.1	
$k_{on(T)}$	log M^{-1} s^{-1} (M^{-1} s^{-1})	8.9 ± 0.3 (7.7×10^8)	8.8 ± 0.4 (7.0×10^8)	7.9 ± 0.3 (8.4×10^7)	8.1 ± 0.4 (1.2×10^8)	7.9 ± 0.1 (7.5×10^7)
$k_{on(R)}$	log M^{-1} s^{-1} (M^{-1} s^{-1})	10.5 ± 0.6 (3.2×10^{10})	10.0 ± 0.6 (1.1×10^{10})	7.4 ± 0.1 (2.5×10^7)	7.5 ± 0.1 (3.3×10^7)	
$k_{off(T)}$	log s^{-1} (s^{-1})	5.2 ± 0.5 (1.6×10^5)	5.7 ± 0.7 (5.2×10^5)	3.4 ± 0.4 (2.6×10^3)	3.9 ± 0.7 (8.7×10^3)	1.5 ± 0.2 (29.5)
$k_{off(R)}$	log M^{-1} s^{-1} (s^{-1})	4.3 ± 0.6 (2.2×10^4)	3.2 ± 0.1 (1.5×10^3)	1.2 ± 0.3 (6.5)	1.0 ± 0.2 (9.6)	

CaM measurements were made on wild-type (WT) and Ca^{2+}-binding site mutant CaMs (EF3,4 and EF1,2) in which only one lobe was functional. Constants are listed in parentheses and as log values ± s.d. above; n_H is the Hill coefficient.

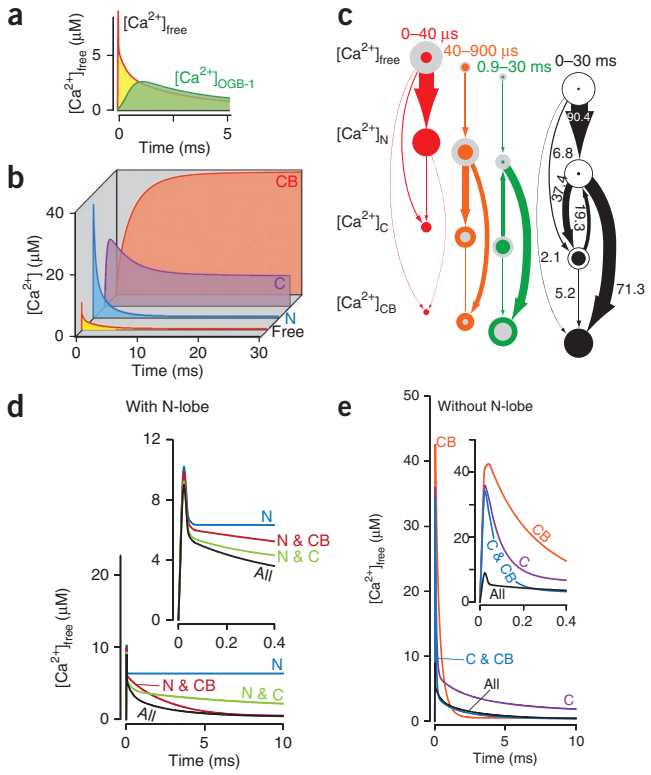

Figure 2 Single-compartment simulations of Ca^{2+} dynamics in a dendritic spine of a hippocampal CA1 pyramidal cell containing 100 μM CaM and 30 μM calbindin. At $t = 0$, $[Ca^{2+}]_{total}$ was rapidly (time constant $\tau = 10$ μs) increased by 50 μM. (**a**) $[Ca^{2+}]_{free}$ and $[Ca^{2+}]$ as it would be measured with 1 yM (10^{-24} M) OGB-1 ($[Ca^{2+}]_{OGB\text{-}1}$). At 20 μs (maximum resolution), $[Ca^{2+}]_{free}$ peaks at 8.8 μM (red line, high peak) because most of the Ca^{2+} is immediately bound. The Ca^{2+} detected by experimentally used concentrations of OGB-1 (green line, low peak) is only a fraction of the initial Ca^{2+} signal. (**b**) The $\Delta[Ca^{2+}]_{total}$ is distributed between the N-lobe (blue, N), the C-lobe (purple, C), calbindin (red, CB) and the $[Ca^{2+}]_{free}$ (red line with yellow fill, Free). (**c**) Movement of Ca^{2+} through the system. The amount of Ca^{2+} flowing between the four states was calculated for three epochs: red, 0–40 μs (peak $[Ca^{2+}]_N$); orange, 40–900 μs (peak $[Ca^{2+}]_C$); green, 0.9–30 ms (end). The $[Ca^{2+}]$ in the different states is represented by the area of the circles (gray area = $[Ca^{2+}]_{start\ epoch}$, colored area = $[Ca^{2+}]_{end\ epoch}$). Numbers indicate percent of $\Delta[Ca^{2+}]_{total}$. Collapsing of all epochs shows the net fluxes during the whole simulation (black). (**d**,**e**) $\Delta[Ca^{2+}]_{total}$ dynamics of the system when it is simulated without various components (N-lobe, C-lobe or calbindin). Components present in the simulations are indicated. (**d**) With the N-lobe present, but with either of the other two components missing, the initial fast buffering stays intact (colored traces versus black traces (no components missing)). (**e**) Without the N-lobe, the initial fast buffering is mostly absent. Whenever calbindin is present (in **d**, N & CB, red; in **e**, C & CB, blue; CB, orange), eventually $[Ca^{2+}]_{free}$ will return to the $[Ca^{2+}]_{final}$ found in the complete model (black). For a more detailed description, see **Supplementary Note**.

not diffuse out of cells[13]. Consistent with this property, much of apocalmodulin is bound to neurogranin (and is released only on Ca^{2+} binding)[7,22]. Moreover, the ability to induce LTP, a phenomenon that depends on CaM, does not rapidly wash out during whole-cell recordings[23], as would be expected if CaM were freely diffusible.

We further analyzed how the different lobes of CaM contribute to fast buffering. Within 40 μs of Ca^{2+} entry, almost 80% of the $\Delta[Ca^{2+}]_{total}$ was bound to the N-lobe. Later, this was redistributed to calbindin and the C-lobe (**Fig. 2b,c**). Consistent with this finding, when calbindin or the C-lobe were taken out of the simulation, the initial fast Ca^{2+} buffering, as indicated by $[Ca^{2+}]_{peak}$, was only marginally affected (**Fig. 2d**). By contrast, when the N-lobe was removed (**Fig. 2e**), the initial fast Ca^{2+} buffering was strongly reduced.

After the initial fast buffering, $[Ca^{2+}]_{free}$ slowly (over 10–30 ms) fell to 350 nM. This decline is noteworthy because a decay with a similar time course was observed in spines and has been attributed to Ca^{2+} pumps[24]. However, our simulation contains no pumps. Therefore, we further examined the mechanism of the slow Ca^{2+} decrease in the absence of Ca^{2+} pumps. When the N-lobe, the C-lobe or both were removed from the simulation, $[Ca^{2+}]_{final}$ was virtually unchanged. However, if we removed calbindin, $[Ca^{2+}]_{final}$ was substantially higher (**Fig. 2d,e**). Thus, calbindin is the main buffer that is responsible for setting $[Ca^{2+}]_{final}$. The overall buffering process is determined by sequential binding events in which the $\Delta[Ca^{2+}]_{total}$ is initially bound to a fast, low-affinity buffer (>90% to the N-lobe of CaM). Then, Ca^{2+} is transferred to an intermediate state (C-lobe of CaM and calbindin) followed by a final stage in which a slow and high-affinity CBP, in this case calbindin, is the main Ca^{2+} buffer (>78% bound; **Fig. 2c**). Thus, reduction in $[Ca^{2+}]$ can be attributed to the movement of Ca^{2+} from fast, low-affinity binding sites to slower, high-affinity sites. Other processes such as diffusion and the action of Ca^{2+} pumps will then determine the final aspects of Ca^{2+} dynamics.

DISCUSSION

Activation of CaM

Our data show that the cooperativity of the two CaM lobes arises from quite different mechanisms. These data improve our understanding of how CaM is activated. Measurements indicate that CaM requires Ca^{2+} binding both in the nanodomain of channels and in the bulk solution of the spine head[25]. In the bulk solution, a modest elevation of Ca^{2+} (1–10 μM) will be sufficient to cause binding to the relatively high-affinity

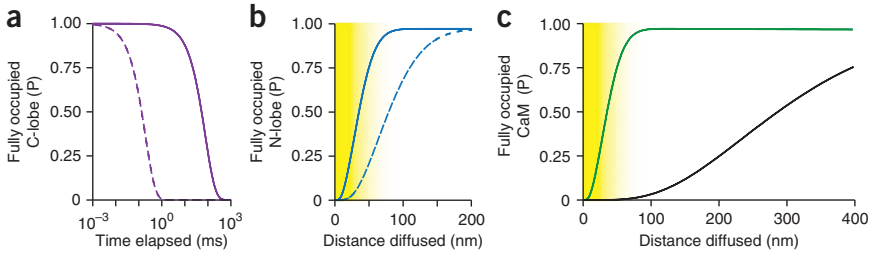

Figure 3 Activation of CaM. (**a**) Probability of a CaM molecule with a fully occupied C-lobe at $t = 0$ having the C-lobe fully occupied by Ca^{2+} as a function of time in the presence of 100 nM $[Ca^{2+}]$ (solid line). The C-lobe remains activated with high probability for tens of ms after it binds the second Ca^{2+}. If the k_{off} of the C-lobe had not decreased upon binding the second Ca^{2+} (dashed line), the lobe would remain activated for <1 ms. This indicates that the switch in k_{off} of the C-lobe is essential for a sustained lifetime of a primed C-lobe. (**b**) Probability of a CaM molecule with no Ca^{2+} bound to the N-lobe at $t = 0$ having the N-lobe fully occupied with Ca^{2+} in a nanodomain with 100 μM $[Ca^{2+}]$ ($D_{CaM} = 50$ nm^2 μs^{-1}, solid line). It is likely that the N-lobe will be activated within the size of a nanodomain. However, if the N-lobe did not have increased k_{on} after binding the first Ca^{2+} (dashed line), the domain size needed for a fully occupied N-lobe would be substantially larger. (**c**) Probability of a CaM molecule becoming fully occupied by Ca^{2+} in a domain with 100 μM $[Ca^{2+}]$. If the molecule has no Ca^{2+} bound at $t = 0$, full activation is unlikely (black line), whereas if the C-lobe is primed (has both binding sites occupied) at $t = 0$, activation within the nanodomain is likely (green line). Yellow areas give approximate size of a nanodomain.

C-lobe. However, if [Ca^{2+}] falls after only one Ca^{2+} binds to the C-lobe, the bound Ca^{2+} will quickly be lost because the extremely fast k_{off} (2.6×10^3 s^{-1}) makes it difficult for this form of CaM to integrate over multiple Ca^{2+} pulses. By contrast, if a second Ca^{2+} binds to the C-lobe, k_{off} decreases to ~1/400×, creating a long-lasting primed pool of CaM (~100 ms; **Fig. 3a**). Further integration could occur when subsequent Ca^{2+} entry creates a high [Ca^{2+}] (100 μM) in the nanodomain; this can load the low-affinity N-lobe of primed CaM (CaM with C-lobe fully occupied; **Fig. 3c**). A freely diffusing CaM molecule will travel out of the nanodomain within tens of microseconds. Therefore, very fast binding of Ca^{2+} to the N-lobe is crucial for two Ca^{2+} ions to bind in the nanodomain. Owing to the high k_{on} for the second binding, there is a >90% probability that a second ion will bind within 1 μs at 100 μM [Ca^{2+}]. Consequently, there is a 75% probability that a totally unoccupied N-lobe will become fully occupied after spending only 12.5 μs in the nanodomain. This time is sufficiently short for a freely diffusing CaM molecule to remain in the nanodomain, as it will travel only ~50 nm in 12.5 μs ($D_{CaM} = 50$ nm^2 μs^{-1} (ref. 26); **Fig. 3b**). If k_{on} did not become elevated owing to cooperativity (that is, it remained at 7.7×10^8 M^{-1} s^{-1}), CaM would probably diffuse out of the nanodomain before a second Ca^{2+} binding could occur (**Fig. 3b**). Thus, the two different types of cooperativity (primarily increasing k_{on} for the N-lobe and primarily decreasing k_{off} for the C-lobe) provide a 'two-step' mechanism for full CaM activation, one within the bulk solution and one within the nanodomain[25], to fully activate CaM (**Fig. 3c**).

In summary, we found that binding of Ca^{2+} to CaM was much faster than to any other known CBP. We have shown that the high concentration of CaM, together with its fast binding kinetics, could largely account for the rapid Ca^{2+} buffering that is observed in dendritic spines. It has generally been assumed that free Ca^{2+} is set by an unknown fast buffer and that CaM responds to this modest Ca^{2+} elevation. Our results provide a very different view: CaM itself acts as the fast buffer, directly intercepting Ca^{2+} before it has a chance to be buffered by other CBPs. This results in highly efficient activation of CaM, resulting in the production of 10–100 times more activated CaM than previously thought (see **Supplementary Fig. 8**). Our results also have implications for other aspects of Ca^{2+} signaling. The transfer of Ca^{2+} from CaM to calbindin (or other CBPs) will itself produce a fall in $[Ca^{2+}]_{free}$, thereby contributing to the overall Ca^{2+} dynamics. Previous work tried to explain this fall solely in terms of Ca^{2+} pumping[24]. A further implication of our findings relates to the observations that cellular levels of CBPs are strongly affected by activity and disease states[27,28]. Our results indicate that such changes in CBPs are effectively gain control mechanisms for transduction that modulates the lifetime of activated CaM.

METHODS

Methods and any associated references are available in the online version of the paper at http://www.nature.com/natureneuroscience/.

Note: Supplementary information is available on the Nature Neuroscience website.

ACKNOWLEDGMENTS

We thank J. Adelman (The Vollum Institute) for purified CaM and mutants of CaM (CaM_{EF12} and CaM_{EF34}), K. Baimbridge (University of Britsh Columbia) for purified calbindin and E.B.S. Faas (Syrinx Design) for help in designing the photodiode pre-amplifier. J.E.L. would like to thank W. Ross and I. Llano for conversations at the Marine Biological Laboratory Woods Hole that led to important insights into this problem. Supported by the US National Institutes of Health (NIH) grants NS027528, NS030549 and the Coelho Endowment to I.M., NIH grant DA027807 to J.E.L. and S.R., and the National Science Foundation grant NSF0642000 to S.R.

AUTHOR CONTRIBUTIONS

G.C.F. was responsible for both theoretical and experimental concepts, experiments, data analysis and writing; J.E.L. and S.R. were responsible for theoretical concepts and writing; and I.M. was responsible for both theoretical and experimental concepts and writing. G.C.F., S.R., J.E.L. and I.M. together developed ideas about how the Ca^{2+} binding properties of multiple Ca^{2+} buffers could explain experimental results in dendritic spines.

COMPETING FINANCIAL INTERESTS

The authors declare no competing financial interests.

Published online at http://www.nature.com/natureneuroscience/.
Reprints and permissions information is available online at http://npg.nature.com/reprintsandpermissions/.

1. Xia, Z. & Storm, D.R. The role of calmodulin as a signal integrator for synaptic plasticity. *Nat. Rev. Neurosci.* **6**, 267–276 (2005).
2. Brown, B.L., Walker, S.W. & Tomlinson, S. Calcium calmodulin and hormone secretion. *Clin. Endocrinol.* **23**, 201–218 (1985).
3. Bers, D.M. Calcium cycling and signaling in cardiac myocytes. *Annu. Rev. Physiol.* **70**, 23–49 (2008).
4. Kubota, Y., Putkey, J.A., Shouval, H.Z. & Waxham, M.N. IQ-motif proteins influence intracellular free Ca2+ in hippocampal neurons through their interactions with calmodulin. *J. Neurophysiol.* **99**, 264–276 (2008).
5. Linse, S., Helmersson, A. & Forsen, S. Calcium binding to calmodulin and its globular domains. *J. Biol. Chem.* **266**, 8050–8054 (1991).
6. Porumb, T. Determination of calcium-binding constants by flow dialysis. *Anal. Biochem.* **220**, 227–237 (1994).
7. Gaertner, T.R., Putkey, J.A. & Waxham, M.N. RC3/Neurogranin and Ca2+/calmodulin-dependent protein kinase II produce opposing effects on the affinity of calmodulin for calcium. *J. Biol. Chem.* **279**, 39374–39382 (2004).
8. Kubota, Y., Putkey, J.A. & Waxham, M.N. Neurogranin controls the spatiotemporal pattern of postsynaptic Ca2+/CaM signaling. *Biophys. J.* **93**, 3848–3859 (2007).
9. Nagerl, U.V., Novo, D., Mody, I. & Vergara, J.L. Binding kinetics of calbindin-D(28k) determined by flash photolysis of caged Ca(2+). *Biophys. J.* **79**, 3009–3018 (2000).
10. Faas, G.C., Karacs, K., Vergara, J.L. & Mody, I. Kinetic properties of DM-nitrophen binding to calcium and magnesium. *Biophys. J.* **88**, 4421–4433 (2005).
11. Faas, G.C., Schwaller, B., Vergara, J.L. & Mody, I. Resolving the fast kinetics of cooperative binding: Ca2+ buffering by calretinin. *PLoS Biol.* **5**, e311 (2007).
12. Berggard, T. *et al.* Calbindin D28k exhibits properties characteristic of a Ca2+ sensor. *J. Biol. Chem.* **277**, 16662–16672 (2002).
13. Sabatini, B.L., Oertner, T.G. & Svoboda, K. The life cycle of Ca(2+) ions in dendritic spines. *Neuron* **33**, 439–452 (2002).
14. Cornelisse, L.N., van Elburg, R.A., Meredith, R.M., Yuste, R. & Mansvelder, H.D. High speed two-photon imaging of calcium dynamics in dendritic spines: consequences for spine calcium kinetics and buffer capacity. *PLoS ONE* **2**, e1073 (2007).
15. Biber, A., Schmid, G. & Hempel, K. Calmodulin content in specific brain areas. *Exp. Brain Res.* **56**, 323–326 (1984).
16. Banay-Schwartz, M., Kenessey, A., DeGuzman, T., Lajtha, A. & Palkovits, M. Protein content of various regions of rat brain and adult aging human brain. *Age (Omaha)* **15**, 51–54 (1992).
17. Muller, A. *et al.* Endogenous Ca2+ buffer concentration and Ca2+ microdomains in hippocampal neurons. *J. Neurosci.* **25**, 558–565 (2005).
18. Neher, E. & Augustine, G.J. Calcium gradients and buffers in bovine chromaffin cells. *J. Physiol. (Lond.)* **450**, 273–301 (1992).
19. Lee, S.H., Rosenmund, C., Schwaller, B. & Neher, E. Differences in Ca2+ buffering properties between excitatory and inhibitory hippocampal neurons from the rat. *J. Physiol.* **525**, 405–418 (2000).
20. Helmchen, F., Imoto, K. & Sakmann, B. Ca2+ buffering and action potential-evoked Ca2+ signaling in dendrites of pyramidal neurons. *Biophys. J.* **70**, 1069–1081 (1996).
21. Meinrenken, C.J., Borst, J.G. & Sakmann, B. Calcium secretion coupling at calyx of held governed by nonuniform channel-vesicle topography. *J. Neurosci.* **22**, 1648–1667 (2002).
22. Putkey, J.A., Kleerekoper, Q., Gaertner, T.R. & Waxham, M.N. A new role for IQ motif proteins in regulating calmodulin function. *J. Biol. Chem.* **278**, 49667–49670 (2003).
23. Otmakhov, N., Griffith, L.C. & Lisman, J.E. Postsynaptic inhibitors of calcium/calmodulin-dependent protein kinase type II block induction but not maintenance of pairing-induced long-term potentiation. *J. Neurosci.* **17**, 5357–5365 (1997).
24. Scheuss, V., Yasuda, R., Sobczyk, A. & Svoboda, K. Nonlinear [Ca2+] signaling in dendrites and spines caused by activity-dependent depression of Ca2+ extrusion. *J. Neurosci.* **26**, 8183–8194 (2006).
25. Lee, S.J., Escobedo-Lozoya, Y., Szatmari, E.M. & Yasuda, R. Activation of CaMKII in single dendritic spines during long-term potentiation. *Nature* **458**, 299–304 (2009).
26. Bloodgood, B.L. & Sabatini, B.L. Neuronal activity regulates diffusion across the neck of dendritic spines. *Science* **310**, 866–869 (2005).
27. Nagerl, U.V. *et al.* Surviving granule cells of the sclerotic human hippocampus have reduced Ca(2+) influx because of a loss of calbindin-D(28k) in temporal lobe epilepsy. *J. Neurosci.* **20**, 1831–1836 (2000).
28. Arnold, D.B. & Heintz, N. A calcium responsive element that regulates expression of two calcium binding proteins in Purkinje cells. *Proc. Natl. Acad. Sci. USA* **94**, 8842–8847 (1997).

ONLINE METHODS

Solutions. All experiments were performed at 35.0 ± 0.1 °C in solutions containing 50 mM KCl, 200 mM HEPES, 50–100 μM Oregon Green BAPTA-5N (OGB-5N, Invitrogen/Molecular Probes) and 3.6–5.6 mM DM-nitrophen (DMn, (4,5-dimethoxi-2-nitrophenyl)-1,2-diaminoethane-N,N,N′,N′-tetrasodium salt, Calbiochem). In selected experiments, the solution also contained calbindin, CaM or one of the mutants of CaM in which the Ca^{2+}-binding sites on either the N-lobe or the C-lobe cannot bind Ca^{2+} (CaM_{EF34} and CaM_{EF12}, respectively). By adding $CaCl_2$, the initial $[Ca^{2+}]_{free}$ of each solution was titrated to be between 250 nM and 1.9 μM (measured with the OGB-5N). Solutions (pH = 7.30 at 35 °C, ionic strength ~130 mM) were freshly prepared before every experiment.

We used OGB-5N because of its fast kinetics of Ca^{2+} binding and unbinding needed for tracking the expected rapid changes in $[Ca^{2+}]$. The properties of the dye (Invitrogen/Molecular Probes, batch lot 29020W) were determined as described[10] (at 35 °C, K_d = 37.9 μM, k_{off} = 33.2 × 10^3 s^{-1}, k_{on} = 8.8 × 10^8 M^{-1} s^{-1} and F_{min}/F_{max} = 39.4).

For each group of experiments, we determined the properties of DMn independently[10,11]. The observed properties of DMn (K_d = 10.0 ± 0.1 nM, k_{on} = 5.2 ± 0.6 × 10^7 M^{-1} s^{-1}, uncaging τ_{fast} = 75 ± 11 μs (67 ± 3%), uncaging τ_{slow} = 1.0 ± 0.1 ms, $k_{off(photoproduct)}$ = 4.6 ± 2.2 × 10^5 s^{-1}) were comparable to published values[10,11]. Also, the [DMn] was determined[29] for each solution independently.

All chemicals were obtained from Sigma-Aldrich unless otherwise stated. Values are expressed as mean ± s.e.m.

Dynamic Ca^{2+} measurements. To measure the dynamics of Ca^{2+} binding to a protein, we used UV-flash photolysis of DMn as described[9–11]. The setup consists of a ~1-μl chamber mounted on a custom-made inverted epifluorescence microscope with a 505-nm dichroic mirror and 510 LP emission filter (Chroma Technology). On top of the chamber, the polished end of a silica multimode optical fiber (Ø 800 μm, 0.37 NA, Thorlabs) was mounted to deliver a flash of UV light (5 ns, 355 nm) from a frequency-tripled Nd:YAG laser (Surelite, Continuum) to photolyze DMn. The power of the UV flash was controlled by the time delay (185–325 μs) of the laser's Pockels cell causing 0.1–8% of the DMn to uncage. To excite the OGB-5N, an argon laser (488 nm, model 95, Lexel) was focused through the epifluorescence pathway with a 20× objective (Fluo20, Nikon), forming a small measurement spot directly in front of the uncaging fiber. Fluorescence was measured with a photodiode (PIN-HR008, UDT Sensors) in the focal plane of the microscope. In spite of using appropriate optical filters and the excitation wavelength of OGB-5N, the high-energy UV flashes still induced brief but large optical transients that saturated the detection system. A custom-built headstage with a fast recovery from overdrive (<10 ns) OP-AMP (OPA699) was used to minimize the duration of the overload (<60 μs). Signals were lowpass filtered (50 kHz, 8-pole Bessel, amplifier Model 440, BrownLee), digitized (200 kHz, PCIO-MIO-16XE-10, National Instruments) and sampled (PC, custom software written in LabView, National Instruments) for offline analysis. For each flash-evoked transient, a fresh ~1-μl droplet of solution was used.

Calmodulin, CaM_{EF12}, CaM_{EF34}, calbindin and determination of protein concentrations. To identify a specific pair of binding sites with specific properties, we used CaM mutants in which aspartate was mutated to alanine in the first Ca^{2+} ligand position of either EF hands 1 and 2 (CaM_{EF12}, C-lobe mutated) or EF hands 3 and 4 (CaM_{EF34}, N-lobe mutated), rendering the mutated EF hand unable to bind Ca^{2+} in the range of the used $[Ca^{2+}]$[30]. Purified CaM and its mutants were a gift from J. Adelman. Purified calbindin was a gift from K. Baimbridge.

To determine the exact protein concentrations used in the experiments, 10–15 μl from each experimental solution was stored at −80 °C for later concentration measurements. The protein concentrations were measured using a detergent-compatible assay based on a folin-phenol reagent (Bio-Rad) with known bovine serum albumin solutions as standards. CaM concentrations were further validated by optical absorbance measurements (Hewlett-Packard 8453). Initial tests with solutions containing DMn and OGB-5N revealed that the colorimetric effect of these compounds was negligible at the concentrations present.

Data analysis and modeling. All data were analyzed using MS Excel (Microsoft) and the ODE solver Berkeley Madonna 8.0 (BM8, UC Berkeley). To determine the kinetic parameters from the recordings, we used a mathematical model built in BM8 that incorporates all the reactions occurring in the experiments (**Supplementary Fig. 1a**). The DMn-uncaging and OGB-5N-signaling parts of this model have been used to determine the properties of DMn and calretinin[10,11]. This model was adapted to simulate the binding of Ca^{2+} to CaM (**Supplementary Fig. 1b**) or calbindin (**Supplementary Fig. 1c**). Spine Ca^{2+} dynamics were modeled using a single-compartment model also built in BM8.

Fitting the Ca^{2+} binding kinetics of CaM and calbindin. To determine the Ca^{2+} binding kinetics of CaM, at least eight variables (x_1 through x_k; for our fits, $k \geq 8$) need to be fitted, leaving too many degrees of freedom to accurately determine all these parameters by fitting single Ca^{2+} transients. We used a procedure[11] that simultaneously fits combined sets of uncaging data obtained under varying experimental conditions (**Supplementary Fig. 1**). This sufficiently constrains the model to yield consistent results. For instance, for wild-type CaM we performed uncaging experiments at seven initial conditions (**Supplementary Fig. 2a–g**) that varied in the initial free $[Ca^{2+}]$ (hence total $[Ca^{2+}]$), total [CaM], total [DMn] and [OGB-5N]. Under each starting condition (a–g), we performed 11–16 uncaging experiments (94 in total), each one with a different amount of uncaging (by varying the energy of the UV flash). To constrain the fits, 32 sets (Set_1 through Set_n; from here on, 'sets' always refer to sets of randomly picked traces) of 14 randomly selected traces from each initial condition a–g were generated. The 32 sets were randomly chosen with the pre-condition that every trace of a specific starting condition a–g was equally represented across the sets (each trace was picked four or five times). Each set of traces was fit (**Supplementary Fig. 2**) with the model and the fit parameters describing the properties of CaM were constrained to be identical for all individual traces within one set. The only parameter that was allowed to vary between traces was the amount of uncaged Ca^{2+}. All 32 results for the fitted values were plotted as a (log-)normal cumulative probability distribution (except for n_H, all parameters were log-normally distributed) and fit to determine the average and the s.d. (**Table 1** and **Supplementary Fig. 3**). For CaM_{EF12} (51 traces, 4 conditions, 26 random sets), CaM_{EF34} (52 traces, 4 conditions, 30 random sets) and calbindin (150 traces, 4 conditions, 30 random sets) the same procedure was followed (**Supplementary Figs. 3** and **4**).

For each fitted trace the correlation coefficient (R) was calculated. For all fitted traces, R was >0.85 for more than 90% (R > 0.9 more than 80%, R > 0.95 more than 50%) of the individual curves. Occasionally, one curve within one set could not be fitted very accurately and had a 0.65 < R < 0.85 which was considered acceptable as the other curves within that set were described with high confidence by the fit.

To further enhance reliability, we actively searched for multiple local minima in the 'error space' and tried to determine the validity of the fit results[11] by implying multiple fitting rounds for each protein (**Supplementary Fig. 5**). In the first rounds of fitting all randomly selected fit sets were fit with a wide variety of starting values for each of the parameters. Thus, each set was fit multiple (j) times within groups (from here on, a 'group' refers to a group of variables within one fit):

$$\left\{ \begin{array}{c} {}^{r}\mathrm{Group}_1 \\ \vdots \\ {}^{r}\mathrm{Group}_j \end{array} \right\} \quad \text{where } {}^{r}\mathrm{Group}_j \in \bigcup_{i=1}^{k} x_{i,j} \qquad (3)$$

where r indicates a collection of groups that are used as starting values for fit round 1 (r = 1), are the results of fit round 1 and are used as starting values for fit round 2 (r = 2) and are the results of fit round 2 (r = 3).

In the first round, the fitting routine is set so that variables can easily make large jumps (**Supplementary Fig. 5**, loose fits). Most fits will find groups of solutions that are comparable for all parameters between the groups (that is, all variables $x_{k,1}$ through $x_{k,i}$ are relatively tightly distributed), which are averaged to one solution group ($^2\mathrm{Group}_1$). Most fits will have as the solution a group of values with one or more parameters that are outliers compared to the commonly found fit values ($^2\mathrm{Group}_2$ through $^2\mathrm{Group}_p$). All groups ($^2\mathrm{Group}_1$ through $^2\mathrm{Group}_p$) are used as starting groups in a second fitting round. In this round all sets are fitted again, but, the fit routine is set so that the parameters only change slowly (**Supplementary Fig. 5**, stiff fits) so the solutions found will

be close to the starting values given. For each group of starting parameters, a collection of groups (one for each fitted dataset) will be obtained:

$$\text{Collection}_j \in \bigcup_{i=1}^{n} {}^3\text{Group}_{j,\,\text{Set}\,i} \tag{4}$$

A collection consists of multiple groups where all (or most) parameters between the groups are comparable and can be described by a single group where the parameters x_k are averages from the x_k values of the multiple groups. Therefore, for each collection j there are k parameters:

$$\bar{x}_{k,j} = \frac{\sum_{i=1}^{n} x_{k,j,\text{Set}\,i}}{n} \tag{5}$$

We found that for all the collections of solutions most parameters were tightly distributed (s.d. < 1 or smaller than one order of magnitude). However, so far, for all but one collection, there is always at least one parameter that has a wide distribution, varying over several orders of magnitude[11]. In these cases, the fits need at least one parameter with a wide distribution to make the fit acceptable. This is an indication that at least one of the other parameters is erroneous, as it forces the system to correct for this error by using a wide distribution of another parameter. Hence, a collection that shows a distribution of several orders of magnitude in one or more parameters was discarded as it must originate from a 'false' minimum in error space. For each experiment, we found only one collection for which all parameters had a tight distribution representing the only valid solution. There might be other sets of such solutions that the fitting routine did not encounter. However, the wide array of starting values in the first rounds cover the whole range of what is physiologically possible. Therefore, unexplored solution sets have parameters of which at least one parameter will fall outside the physiological range.

Stability of the model. By using the procedure described above, we found that most fits will find very similar solutions for most or all parameters regardless of the initial starting values. From this we conclude that small deviations in the values of these parameters will not cause large changes in the outcome of the model. However, in our model we defined many of the parameters as constants. These parameters ($[Ca^{2+}]_{rest}$, $[protein]_{total}$, rates of (un)binding and uncaging of DMn, rates of (un)binding of the photoproducts of DMn, rates of (un)binding of OGB-5N and the F_{ratio} of ORB-5N) were determined in independent experiments. We tested whether small perturbations of these constants would have a significant influence on the results of our modeling. Two sets of curves of the wild-type data were randomly picked and were re-fitted with the same model except that each of the above constants was randomly changed by +5%, 0% or −5%. This was repeated 11 times, giving 24 sets of fitted parameters that varied owing to the random variations of the constants. We found that the fit results obtained in this manner varied similarly to or less than the original fit results of all data (**Supplementary Fig. 6**). Overall, we conclude that small deviations of any of the parameters considered to be constant will not cause large changes in the outcome of the model (that is, there are no large nonlinear effects in the explored area of the parameter space).

29. Kaplan, J.H. & Ellis-Davies, G.C. Photolabile chelators for the rapid photorelease of divalent cations. *Proc. Natl. Acad. Sci. USA* **85**, 6571–6575 (1988).
30. Peterson, B.Z., DeMaria, C.D., Adelman, J.P. & Yue, D.T. Calmodulin is the Ca^{2+} sensor for Ca^{2+} -dependent inactivation of L-type calcium channels. *Neuron* **22**, 549–558 (1999).

doi:10.1038/nn.2746